Target fragmentation of Au and Th by 2.6 GeV protons

K. Sümmerer, W. Brüchle, D. J. Morrissey,* M. Schädel, B. Szweryn,† and Yang Weifan‡
Gesellschaft für Schwerionenforschung, D-6100 Darmstadt, Federal Republic of Germany
(Received 09 July 1990)

Target residues from the reaction of 2.6 GeV protons with gold and thorium nuclei have been studied with radiochemical techniques. Chemical separations were used to enhance the sensitivity for detecting target residues in the near-target region. These data are compared to a new empirical parametrization of the mass and charge yields of fragmentation, or spallation, products based on a comprehensive analysis of data in the literature. Data include results from both projectile and target fragmentation studies. The new near-target residues provide significant new insight into the variation of the cross sections of products near in mass to the target (or projectile). The results of this study and the empirical description are compared to the internuclear-cascade model of these reactions.

I. INTRODUCTION

The investigation of target residues from proton- or heavy-ion-induced reactions at relativistic energies has been a field of active research—mainly with radiochemical techniques—for at least the last two decades. The empirical systematics that have been established in the course of this work and their interpretation have been the subject of several review articles (see, e.g., Refs. 1 and 2). From these reviews one can draw the conclusion that the basic features of target fragmentation, sometimes also called "spallation," are well understood: heavy fragments such as those in the present study arise from *peripheral* collisions of heavy ions or relativistic protons with the target nucleus. These so-called "spectators" of the reaction are excited primary fragments which then decay into the final fragments by a sequence of evaporation steps. The spectrum of residual nuclei seems to be determined to a large extent, but not fully, by the evaporation process. In the context of the present work two other observations are particularly relevant: (i) the distribution of target residues becomes approximately energy independent above a certain threshold of the projectile total kinetic energy; (ii) the cross sections for a specific near-target fragment produced in proton- or light-ion-induced reactions differ only by a constant factor that is close to the ratio of the total reaction cross sections. The terms "limiting fragmentation" and "factorization" have been coined for the latter two observations, respectively.[2]

Recently, the systematic behavior of target-fragmentation cross sections has received renewed interest from experimenters interested in studying the inverse process of projectile fragmentation. Since projectile fragments are almost at rest in the *projectile* reference frame, just as the target fragments are nearly at rest in the laboratory frame, they must be studied with physical detection techniques that were not applicable to the slow target fragments (where radiochemical techniques have dominated). The possibility of producing intense secondary beams of single exotic isotopes with projectile-fragment isotope separation techniques at relativistic energies[3,4] has especially stimulated interest and experimental effort in this area, e.g., the construction of a Projectile-Fragment Separator, FRS, at GSI.[5]

The predictions of the intensities of such secondary beams have relied on the systematics of fragmentation cross sections. Such systematics are primarily empirical and are cast in analytical formulas like the one suggested by Rudstam.[6] Although this original work has been extended by many authors, the general validity of most of these descriptions, beyond application to a limited range of fragments, has not been established. In particular, it is still difficult to predict the cross sections of the fragmentation products of heavy nuclei. This is mainly due to the fact that experimental data for such fragments are only available from radiochemical studies of target fragmentation and are therefore sparse.

The present study has been undertaken to provide some pivotal data points at the upper end of the chart of nuclides for an empirical parametrization of fragmentation yields. We have measured target-fragment cross sections from the interaction of 2.6 GeV protons with gold and thorium targets with radiochemical techniques. These two target nuclei were chosen because they represent heavy nuclei with high and low fission barriers, respectively, thus allowing us to estimate the importance of fission competition in the production of trans-lead fragments from Th and U targets. Although suitable radiochemical yields are necessarily scattered in the chart of the nuclides as the technique requires nuclei with suitable decay characteristics, they still represent the only present-day source of individual-isotope formation cross sections at medium to high Z and A. In our experiment, special care was taken to obtain a large number of *independent* cross sections because such values are needed to fix the position of the primary (i.e., pre-β-decay) yield curves. We have performed chemical separations of several elements immediately after the bombardment to cut

the β-decay chains as early as possible and to improve the detection sensitivity for low-yield isotopes.

Sections II and III of the present paper contain details of the experimental procedures and the list of cross sections obtained. In Sec. IV we present a new empirical parametrization of fragmentation cross sections based primarily on the large amount of experimental data in the literature. Our goal was to obtain a formula to calculate the fragmentation cross section of an arbitrary product nucleus in any fragmentation reaction provided the limiting conditions are fulfilled. In particular, we have developed a parametrization that takes into account the influence of the proton- or neutron-excess of the target. This description is also confronted with the results of the present experiment. The agreement is good except the description of near-target residue cross-sections from heavy targets requires important modifications of the formulas. Finally, we include calculations with the internuclear-cascade-plus-evaporation model of Yariv and Fraenkel[7] of the fragmentation process to obtain some insight into the physical nature of the reaction. We will demonstrate that the microscopic calculations and empirical systematics at least qualitatively yield similar results but the numerical accuracy is better for the empirical description.

II. EXPERIMENTAL PROCEDURES AND DATA ANALYSIS

The irradiations were performed with an external beam of 2.6 GeV protons from the SATURNE synchrotron at Saclay. The beam was delivered to the targets in bursts of $\approx 5 \times 10^{11}$ protons each with a repetition rate of $0.3 s^{-1}$. The size of the beam spot at the target position was monitored on-line with wire chambers and off-line by the autoradiography of some irradiated targets. The variation of the intensity of the incident proton beam with time was recorded with a neutron counter placed near the target. The integral proton flux was recorded in relative units by the SATURNE computer control system and was later converted to the absolute number of protons passing through the target (see below).

Targets of $\approx 80 mg/cm^2$ Au and $\approx 50 mg/cm^2$ Th were irradiated together with aluminum foils of $\approx 5 mg/cm^2$. The latter were used to determine the proton flux via $^{27}Al(p,X)^{22,24}Na$,^{7}Be monitor reactions. To avoid scattering-out losses, each of the Al targets was the center foil of a stack of three identical foils. Similarly, the gold and thorium target foils were surrounded by foils of the same material with thicknesses of $\approx 10 mg/cm^2$. The target foil stacks were covered with 75 μm Mylar foils and separated from each other by approximately 1 cm. Details of the individual irradiations are listed in Table I.

After the irradiations, the central target foil of each stack was removed and transferred to a chemistry laboratory where an $\approx 1 cm^2$ portion of the target material was dissolved. Chemical fractions of the elements Au, Pt, Os, Ir, Ta, and Hf were prepared from the gold targets of runs 1 and 2. Two rare-earth fractions comprising the elements from Lu to Er and from Gd to Sm, were also extracted. The gold target of run 3 was measured without chemical separation in order to obtain the chemical yields of runs 1 and 2. Only Tl and Au fractions have been prepared from the thorium target. Details of the chemical separation procedures can be found in a separate publication.[8] Typically, the samples were ready for measurement between one and six hours after the end of an irradiation.

TABLE I. Irradiation parameters for the irradiation of Au and Th targets with 2.6 GeV protons.

Run No.	Target	Thickness (mg/cm^2)	Irradiation time (min)	Proton flux (particles)
1	Au	79.2	116	6.62×10^{14}
2	Au	79.4	636	3.66×10^{15}
3	Au	79.5	446	2.64×10^{15}
4	Th	51.4	61	3.34×10^{14}

The samples were assayed at Saclay with two unshielded Ge(Li) detectors for short-lived activities. About 12 hours after the end of the last irradiation, the samples were transferred to GSI, where measurement with eight shielded Ge(Li) detectors continued for several months. The resulting decay curves of a large number of γ peaks were analyzed in the usual way to obtain the activities of all identifiable isotopes as a function of time after the chemical separation. Isotopic assignments were based on a computerized version of the γ-ray catalog by Reus, Westmeier, and Warnecke.[9] The decay rates of the individual isotopes were converted to formation cross-sections taking into account the incident proton flux, the irradiation history, and the chemical yields of the respective fractions.

III. RESULTS

A. Cross sections for gold targets

The cross sections resulting from the runs with Au targets are compiled in Table II. Absolute values have been determined by normalizing the results for several long-lived isotopes observed in run 3, where no chemical separations have been performed, to those from Kaufman *et al.*[10] at a proton energy of 3 GeV. Such a normalization determined the proton flux for run 3 listed in Table I and, subsequently, the proton flux of the other irradiations through the relative numbers of accelerated protons given by the SATURNE control system. The resulting values were found to be consistent with the flux obtained from an analysis of the monitor reactions $^{27}Al(p,X)^{7}Be$, $^{27}Al(p,X)^{22}Na$, and $^{27}Al(p,X)^{24}Na$ based on the interpolated cross sections from the compilation of Tobailem *et al.*[12] of 8.7 mb, 11.6 mb, and 9.4 mb, respectively.

Because chemical separations were performed in runs 1 and 2, the chemical yields had to be determined before calculating the cross sections. This was done by comparing cross sections of long-lived isotopes to those of the same isotopes obtained with the unseparated target. When necessary, corrections for different irradiation histories were applied. This procedure was not applicable to the Ta fraction since no long-lived isotopes were observed in run 3. As there are no data available in the literature for tantalum isotopes we have chosen to normalize the cumulative cross sections for ^{175,176,177}Ta to calculated values from the empirical parametrization which will be described in Sec. IV.

The cross sections listed in Table II are for the most part either independent (long-lived precursors or shielded isotopes) or cumulative (short-lived precursors). In some cases the precursor half-lives were comparable to the time elapsed between the end of irradiation and the chemical separation and thus the measured cross sections were not fully cumulative. In those cases (marked with superscript "c" in Table II) we have used the measured precursor cross-section and the irradiation history to convert the measured partially cumulative to fully cumulative cross sections.

The cross sections determined by other authors at proton energies of 3 GeV, 6 GeV (Ref. 10), and 11.5 GeV (Ref. 11) are also given in Table II. Of those, most of the data at 3 GeV were used to normalize our data and, thus, are not an independent check, but serve to illustrate the degree of agreement between two sets of data. A more recent measurement with 12 GeV protons has been performed by Asano *et al.*[13] Their results are in good

TABLE II. Summary of target-fragment cross sections for the reaction of protons with gold targets from this work in comparison with previous results. The kinetic energy of the incident protons is indicated in the different columns.

Isotope	Half-life	This work (2.6 GeV)		3 GeV[a]	6 GeV[a]	11.5 GeV[b]
		σ_{ind} (mb)	σ_{cum} (mb)	σ (mb)	σ (mb)	σ (mb)
^{198}Au^{g}	2.7 d	3.95±1.44				
^{196}Au^{g}	6.2 d	74.4±5.2		76±7[i]	73±7[i]	75±5[i]
^{196}Au^{m}	9.7 h	3.04±0.20				
^{195}Au	183 d		26.9±2.7			
^{194}Au	39.5 h	29.6±2.6		30.3±2.5[i]	28.8±2.3[i]	29.4±2.2[i]
^{193}Au	17.7 h		17.5±1.7			
^{192}Au	5.03 h		16.1±3.3			
^{191}Au	3.18 h		17.1±4.2			
^{195}Pt^{m}	4.02 d	7.31±0.83				
^{191}Pt	2.8 d		16.7±2.4			
^{189}Pt	11 h		25.3±4.6			
^{188}Pt	10.2 d		19.8±2.3	21.8±1.7	18.9±2.0	20.7±1.4
^{195}Ir^{m}	3.8 h	1.75±0.29				
^{194}Ir^{g}	19.2 h	0.86±0.15				
^{192}Ir^{g}	74 d	1.63±0.19		2.13±0.20[i]	2.16±0.20[i]	2.45±0.16[i]
^{190}Ir^{g}	12.1 d	2.16±0.26		3.69±0.35[i]	3.80±0.42[i]	4.06±0.30[i]
^{190}Ir^{m}	3.1 h	1.26±0.24				
^{188}Ir	41.5 h	5.44±0.79		6.5±1.0[i]	6.3±1.2[i]	6.5±1.1[i]
^{187}Ir	10.5 h		29.6±3.5			
^{186}Ir^{b}	15.8 h	12.3±2.0				
^{185}Ir	14 h		16.3±2.0			
^{184}Ir	3.0 h		15.5±2.8			
^{191}Os^{g}	15.4 d	0.68±0.14				
^{185}Os	94 d		25.8±2.5[c]	26.1±2.2	22.1±2.3	21.8±1.7
^{183}Os^{g}	13 h		21.9±3.5[c]			12.0±2.0
^{183}Os^{m}	9.9 h		22.1±1.1			10.0±1.7
^{182}Os	21.6 h		37.6±4.4	22.5±3.0		19.0±2.0
^{186}Re^{g}	90.4 h	0.33±0.05				
^{184}Re^{g}	38 d	0.90±0.14				
^{182}Re^{g}	64 h	1.48±0.26				
^{182}Re^{m}	12.7 h	3.0±1.0				
^{181}Re	20 h		39.5±7.6	22.4±2.1	17.7±2.5	
^{182}Ta	115 d	0.064±0.004				
^{177}Ta	56.5 h		18.0±0.9			
^{176}Ta	8.08 h		26.8±2.7			
^{175}Ta	10.5 h		28.1±1.2			
^{173}Ta	3.6 h		22.9±4.2			

TABLE II. (*Continued.*)

Isotope	Half-life	This work (2.6 GeV)		3 GeV[a]	6 GeV[a]	11.5 GeV[b]
		σ_{ind} (mb)	σ_{cum} (mb)	σ (mb)	σ (mb)	σ (mb)
^{173}Hf	23.9 h		20.5±1.6 [c]			
^{172}Hf	1.87 a		16.5±4.9	18.8±1.5	14.7±1.6	16.3±1.3
^{171}Hf	12.1 h		18.9±2.6			
^{170}Hf	16 h		21.2±1.9			
^{174}Lu	3.31 a	0.04±0.02				
^{172}Lu	6.7 d	0.307±0.046				
^{171}Lu	8.2 d		23.7±2.9 [c]	20.6±1.5	15.7±1.3	17.3±1.1
^{170}Lu	2.0 d		23.4±2.9 [c]	17.3±1.5	13.3±1.2	19.1±1.3
^{169}Lu[g]	1.42 d		31.0±3.1			
^{169}Yb	30.7 d		46.0±2.1 [c]			17.5±1.8
^{166}Yb	56.7 h		23.1±1.0			
^{168}Tm	93.1 d	0.07±0.02				
^{167}Tm	9.24 d		28.5±0.9	18.2±1.7	14.0±1.3	15.5±1.1
^{166}Tm	7.7 h		24.4±0.7 [c]			
^{165}Tm	30.1 h		27.4±0.8			
^{156}Tb[g]	5.35 d	0.61±0.03				
^{153}Gd	242 d	2.71±0.48				
^{149}Gd	9.4 d		19.7±1.0	22.0±2.0	15.4±1.4	15.6±1.0
^{147}Gd	38 h		15.1±0.8			
^{146}Gd	48.3 d		15.5±0.9	17.3±1.5	12.3±1.0	11.5±0.8
^{148}Eu	55.6 d	0.475±0.025				0.58±0.06 [i]
^{146}Eu	4.61 d	2.61±0.19				
^{145}Eu	5.94 d		13.1±0.9	18.5±1.7	13.8±1.2	13.0±0.8

[a] Kaufman *et al.*(Ref. 10).

[b] Kaufman *et al.*(Ref. 11).

[c] Corrected to represent fully cumulative yield.

[i] Independent yield.

agreement with those of Ref. 11. The data at the higher energies are generally in very good agreement with the lower energy data and support the hypothesis of "limiting fragmentation," i.e., the energy-independence of isotopic cross sections at relativistic energies.[2]

B. Cross sections for the thorium target

As noted before, an irradiation of the thorium target with 2.6 GeV protons (run 4 in Table I) was undertaken to obtain cross sections from a much more fissile nucleus in a mass region where experimental data are scarce. Compared to the irradiations of gold targets, the measurements were far less complete as only thallium and gold fractions were extracted after dissolving the thorium target.[8] These two elements were selected because they can be easily separated with high yields. Moreover, the decay properties of several isotopes are favorable for radiochemical experiments and can give a number of independent or only partially cumulative cross sections, especially if fast chemical separations are performed.

Absolute cross sections from this experiment were calculated in the same manner as those for gold targets except for the determination of chemical yields. In the present case, ≈ 10 mg of Tl and Au carriers were added before the chemical separations and the chemical yield could be determined simply by weighing. The resulting efficiencies were 73 ± 3 % and 76 ± 3 % for Tl and Au, respectively.

Table III lists the cross sections obtained for Tl and Au

TABLE III. Target-fragment cross sections for thallium and gold isotopes produced in the reaction of 2.6 GeV protons with ^{232}Th.

Isotope	Half-life	σ_{ind} (mb)	σ_{cum} (mb)
^{202}Tl	12.23 d	0.039±0.002	
^{201}Tl	73.1 h		0.268±0.014
^{200}Tl	26.1 h		0.214±0.009
^{199}Tl	7.42 h		1.84±0.10
^{198}Tl[g]	5.3 h		1.62±0.16
^{197}Tl	2.84 h		5.52±0.22
^{196}Tl[g]	1.8 h		1.56±0.08
^{196}Tl[m]	1.4 h		1.15±0.04
^{195}Tl	1.13 h		5.97±0.08
^{199}Au	3.14 d	0.018±0.004	
^{198}Au[g]	2.7 d	0.017±0.001	
^{196}Au[g]	6.2 d	0.030±0.001	
^{195}Au	183 d	0.52±0.07	
^{194}Au	39.5 h	0.10±0.004	
^{193}Au	17.7 h		0.89±0.08
^{192}Au	5.03 h		1.06±0.10
^{191}Au	3.18 h		3.99±0.17

isotopes from the thorium target. We have measured the independent cross sections, column 3 of Table III, for the isotopes ^{202}Tl and $^{194-196,198,199}$Au. The experimental cross sections of the other isotopes include varying precursor contributions and are listed in column 4 of Table III. Since we have not measured the respective precursor cross sections, the precursor contributions cannot be subtracted as was done for the gold target (Table II).

IV. DISCUSSION

A. Energy dependence of fragmentation cross sections

Since the present study is aimed at a systematic investigation of fragmentation cross-sections in the limiting-fragmentation regime, the question of whether limiting fragmentation is reached at 2.6 GeV proton energy should be addressed first. According to the excitation functions measured for the reaction p+Au by Kaufman *et al.*,[10,11] a proton energy of ≈ 3 GeV should be just at the onset of energy-independence for the cross sections of most of the heavy fragments. The same conclusion can be drawn from an analysis of the energy-dependence of the slope of the mass-yield curve[16] for copper fragmentation. Our results comply with these previous observations. Several *independent* cross sections are shown in Fig. 1 as a function of incident proton energy between 1 and 300 GeV. As suggested by the horizontal lines, fitted to the high-energy data (2.6 GeV to 300 GeV), the scatter of the individual values is of the same order of magnitude as a possible energy dependence of the cross sections. This holds for fragments close in mass to the target (Ir) and those further removed (^{148}Eu). We conclude that for all practical purposes our results are within errors identical to those at higher energies.

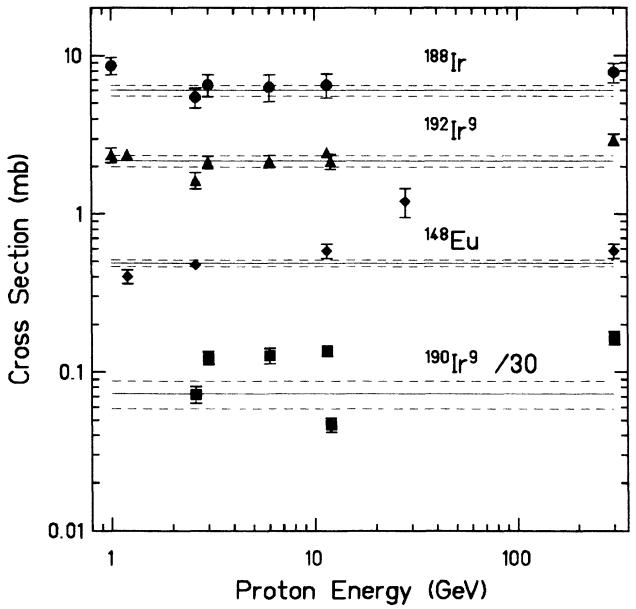

FIG. 1. Independent cross sections of several isotopes produced in the reaction of GeV protons with ^{197}Au. Data at 2.6 GeV energy are from this work. The other data have been taken from Refs. 10 and 11 except for those at 1.2 GeV (Ref. 14), 12 GeV (Ref. 13), and 28 GeV (Ref. 15). Data for ^{190}Ir^{g} have been divided by a factor of 30 for clarity. The horizontal lines indicate the weighted mean of the high-energy data (2.6 GeV–300 GeV) and the corresponding error band.

B. Comparison with heavy-ion induced reactions

As mentioned in the Introduction, present and envisioned radioactive-beam facilities have revived the interest in the prediction of fragmentation cross-sections. To predict the intensities of radioactive beams produced by projectile fragmentation one needs, in general, the cross sections for a heavy-ion beam on a light target, which—in the target rest frame—corresponds to the target-fragment cross section with a light-ion beam. Since only relatively few data have been measured for light-ion beams, particularly for heavy targets, the question arises if the data obtained with intense beams of GeV protons can be used to complement the much scarcer data obtained with heavy-ion beams (with generally poorer statistical accuracy). Previous comparisons of proton- and heavy-ion-induced target-fragmentation cross-sections at similar projectile kinetic energies in the GeV range have shown that the shape of the respective isotope distributions for ^{nat}Cu and ^{nat}Ag targets[16,17] are not different within experimental errors, i.e., data obtained with protons can be scaled to match those obtained with heavy ions. In the case of heavy targets, large error bars and poor statistics have hampered comparisons up to now. In Fig. 2 we show the result of such an analysis for our experiment with gold as a target. In the upper part of this figure, the ratios of *independent* cross sections from the reaction of 8 GeV ^{20}Ne with Au (Ref. 18) to our results from Table II are shown as a function of fragment mass. Although not many isotopes have been observed with high precision in both experiments, the ratios are compatible with a constant value somewhat below a factor of 2. This value is smaller than the calculated ratio of the total reaction cross-sections[19] for Ne+Au and p+Au [dashed line at 2.45 in Fig. 2(a)], which would be suggested from the scaling of the proton-induced reactions with the total reaction cross-section, σ_R, as discussed below (Sec. IV A). The same conclusion, again with poor statistics, can be drawn from a similar analysis of previously published heavy-fragment cross-sections from the reactions of 8 GeV ^{20}Ne with ^{181}Ta (Ref. 18) and of 12 GeV protons with ^{181}Ta (Ref. 13) [see Fig. 2(b)]. However, in both cases, the ratio calculated with our empirical parametrization of fragmentation cross sections—derived from experimental data with a much wider span of projectile and target masses (see Sec. IV A)—reproduces the data well. We conclude that the scaling behaviour observed for light- and medium-mass targets holds also for heavy targets and that proton-induced reactions in

the limiting-fragmentation regime can be used to produce fragment isotope distributions that should be proportional to those produced in heavy-ion-induced reactions.

C. Empirical parametrization of fragmentation cross sections

The radiochemical methods used in the present experiment have the advantage that many fragments are uniquely identified with respect to A and Z. On the other hand, a much larger number of isotopes cannot be detected because they are either stable or have unfavorable decay characteristics. It is therefore important to develop a smooth analytical formula to describe the yield distributions and interpolate between the measured data points. The experimental data points serve to pin down the parameters of the formula by a fitting procedure. Remembering the current interest in the systematics of fragmentation cross sections, we aimed at a formula which was not only to reproduce the results of the present experiment, but also the large number of cross sections from the literature to a reasonable extent. If such a formula can be given as a function of few parameters like the mass and charge numbers of projectile, target, and fragment, it can then also be used to predict cross sections for arbitrary reaction partners and fragments.

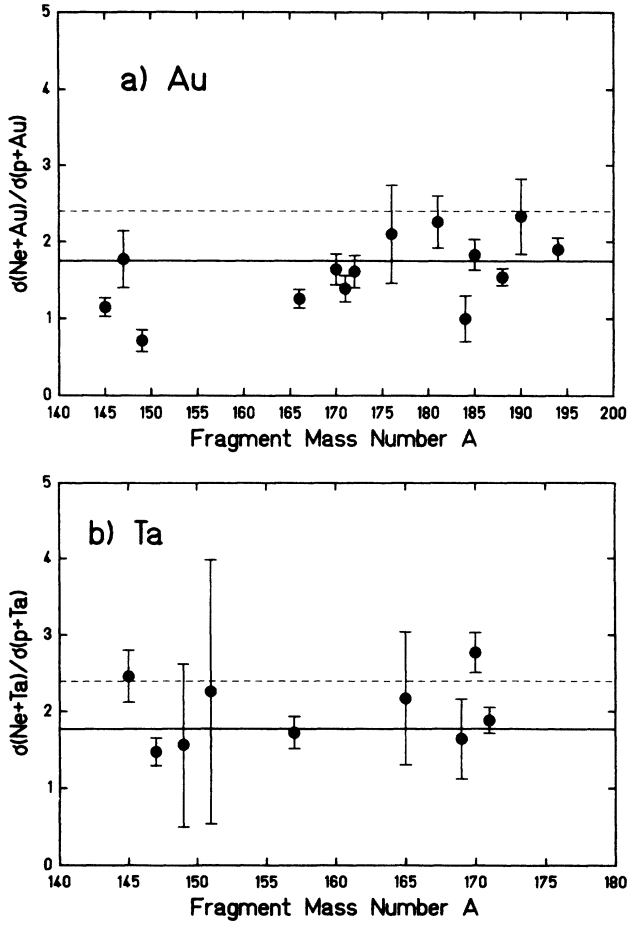

FIG. 2. Ratio of isotopic cross sections for light-ion- and proton-induced reactions plotted as a function of fragment mass: (a) for the reaction of 8 GeV ^{20}Ne and 2.6 GeV protons with ^{197}Au, (b) for the reaction of 8 GeV ^{20}Ne and 12 GeV protons with ^{181}Ta. Data for the Ne projectile have been measured by Morrissey *et al.*(Ref. 18). The proton data in the upper part are from this experiment (Table II), in the lower part from the work of Asano *et al.*(Ref. 13). The dashed line indicates the ratio of total reaction cross-sections according to Kox *et al.*(Ref. 19) for the respective systems. The full line represents the ratio calculated according to our empirical parametrization of fragmentation cross-sections (see text).

Analytical formulas for fragmentation reactions were first suggested by Rudstam[6] and later elaborated by many other authors, notably by Silberberg *et al.*[20,21] The form of the yield distribution as a function of fragment mass and charge $\sigma(A,Z)$ is conventionally written as

$$\sigma(A,Z) = Y(A)\,\sigma(Z_p - Z) = Y(A) n \exp(-R|Z_p - Z|^U)\,. \tag{1}$$

The first term $Y(A)$ represents the mass yield, i.e., the sum of the isobaric cross sections with mass A. The second term describes the charge dispersion, the distribution of elemental cross sections with a given mass around its maximum, Z_p. The shape of the charge dispersion is controlled by the width parameter, R, and the exponent, U. The factor n simply serves to normalize the integral of the charge dispersion to unity.

The parameters for Eq.(1) given by Kaufman *et al.*[11] for the p+Au reaction are a convenient starting point for the present work. However, it became clear that this choice of parameters could reproduce many of our data points only poorly, in particular yields of fragments close to the target. Moreover, it would not be useful to have a set of parameters that was valid only for a certain target-projectile combination. Similar difficulties occured with the more general formula given by Silberberg *et al.*[20,21]

In order to arrive at rather simple equations that contain the global trends of the yield distributions, our empirical formula was restricted to *heavy-fragment* production ("spallation" in terms of the classification suggested by Hüfner [1]). That is, multi-fragmentation, intermediate-mass fragments, and fission products were excluded from the scope of the description. We have also restricted ourselves to fragments from nuclei heavier than $A \approx 40$. By inspection of, e.g., the data of Olson *et al.*[23] one can see that isotope distributions from very light nuclei, e.g., ^{12}C or ^{18}O, cannot be approximated by the smooth functions that describe heavier nuclei. In the following section we will discuss in detail functional form and parameters for the different terms of Eq.(1).

(Very recently, Webber, Kish, and Schrier[22] have published an extensive study of the fragmentation of nuclei up to ^{56}Fe on light targets and suggested a new formula to calculate isotopic cross sections for nuclei with

$4 \leq Z \leq 28$ and $7 \leq A \leq 60$ from hydrogen targets including bombarding-energy dependent terms. Similar to Silberberg *et al.*,[20,21] the objective of their work is to describe *precisely* cross sections relevant to cosmic-ray propagation. Since our aim, however, is to obtain an *approximate* formula that allows to calculate isotopic yields from all kinds of target-projectile combinations—including very heavy targets—we have not attempted to include these very recent results in the present work.)

1. Mass yield curves

Most authors have based their choice for the functional form of the mass yield curve on the observation that the total isobaric cross section of heavy target fragments decreases exponentially with increasing distance from the target mass, A_t. Abul-Magd, Friedman, and Hüfner[24] have shown that for relativistic-proton-induced reactions one obtains the following function under very simple assumptions for the reaction mechanism:

$$Y(A) = \sigma_R P(A_t) \exp[-P(A_t)(A_t - A)] \qquad (2)$$

which is very similar to the high-energy limit of the Rudstam formula[6]. In this equation, σ_R is the total reaction cross-section in millibarns, which for proton-induced reactions is taken from the work of Kox *et al.*[19] For limiting fragmentation, the slope parameter $P(A_t)$ depends only on the target mass and not on the bombarding energy.[16] We have fitted $P(A_t)$ to data from the literature for the target fragmentation reactions of p+V (Ref. 25), p+Cu and C+Cu (Ref. 16), p+Ag and C+Ag (Ref. 17), and p+Au from Refs. 10, 11, and this work. We have also included the data from the projectile-fragmentation of Ar+C (Ref. 26). (As mentioned above, the data of Webber, Kish, and Schrier[22] have not been included in the fit. Within the accuracy of the present study, their data are in good agreement with previous work. Their results could, however, be included in a future revision of our formula.) The different experimental slope parameters are shown in Fig. 3 together with the fitted curve (full line) written as

$$\ln P(A_t) = -7.57 \times 10^{-3} A_t - 2.584. \qquad (3)$$

Also shown by the dotted curve in Fig. 3 is the functional form suggested by Silberberg, Tsao, and Letaw,[21] $P(A_t) = 2.51 A_t^{-0.96}$. These curves are very similar but Eq.(3) matches better the small slope derived from the data of Viyogi *et al.*[26] for the Ar+C system.

While Eq.(2) reproduces well the fragmentation data for reactions induced by protons, it does not give the proper scaling for heavy-ion induced reactions. This is due to the peripheral nature of fragmentation reactions; the mass yields and (recall the discussion of scaling in Sec. IV B) the isotopic cross sections depend on the sum of the target and projectile radii rather than the square of the sum contained in the factor σ_R from Ref. 19. Experimental evidence for this scaling law has been provided by

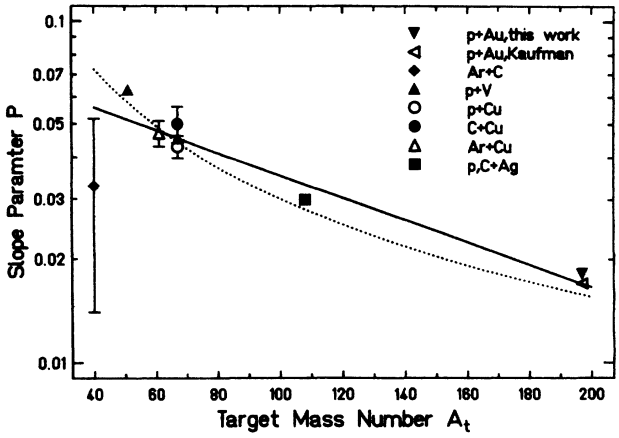

FIG. 3. Slope parameter P of the mass yield curve according to Eq.(2) plotted as a function of target mass. The data points have been obtained by analyzing data for ^{40}Ar as a projectile (Ref. 26) and targets of ^{51}V (Ref. 25), ^{nat}Cu (Ref. 16), ^{nat}Ag (Ref. 17), and ^{197}Au (Ref. 10 and this work). The full line is our exponential fit to the data [Eq.(3)], the dotted line represents the function suggested by Silberberg, Tsao, and Letaw (Ref. 21).

Olson *et al.*[23] for ^{18}O fragmentation and more recently by Hill *et al.*[27] for ^{59}Co, ^{89}Y, and ^{197}Au fragmentation. (Note that Cumming *et al.*[16] found a scaling proportional to σ_R for proton- and ^{40}Ar-induced reactions with ^{nat}Cu, but this at variance with the other experiments cited above.[23,27]) For this reason, we have chosen to substitute, for heavy-ion induced reactions, the factor σ_R in Eq.(2) with

$$\sigma'_R = 450(A_p^{1/3} + A_t^{1/3} - 2.38) \text{ mb}, \qquad (4)$$

where A_p and A_t denote the projectile and target mass numbers, respectively.

The reduced values of σ'_R for the interaction of ^{18}O with various targets[23] and for the interaction of ^{59}Co, ^{89}Y, and ^{197}Au with various projectiles[27] are shown in Fig. 4 as a function of $A_p^{1/3}+A_t^{1/3}$. In this figure, we show reduced values of σ'_R (or "projectile factors" in terms of a factorization analysis[2,23]). They are obtained simply by dividing by σ'_R for ^{12}C-induced reactions. The figure demonstrates that Eq.(4) represents a reasonable description of the scaling of fragmentation cross-sections as a function of the size of the interacting nuclei. Deviations are observed for ^{18}O fragmentation at the largest target mass numbers. This suggests to introduce an overlap factor that varies with A_p and A_t instead of the constant value of 2.38 used in Eq.(4). In view of the large error bars for the heavier systems, however, we were unable to derive such a parametrization for arbitrary systems.

2. Charge dispersion curves

Given Eq.(1), in order to specify the distribution of nuclear charges, Z, for a given fragment-mass number, A, the three parameters R, Z_p, and U must be known.

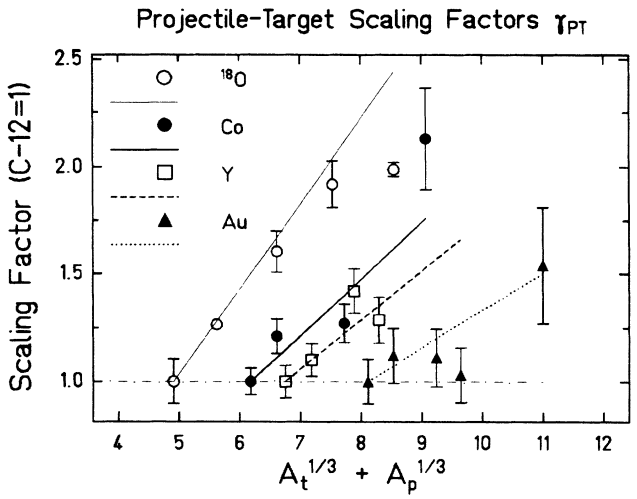

FIG. 4. Projectile-target scaling factors according to Eq.(4) normalized to the corresponding values for ^{12}C. The symbols represent data points for ^{18}O projectile fragmentation[23] and for ^{59}Co, ^{89}Y, and ^{197}Au target fragmentation (Ref. 27).

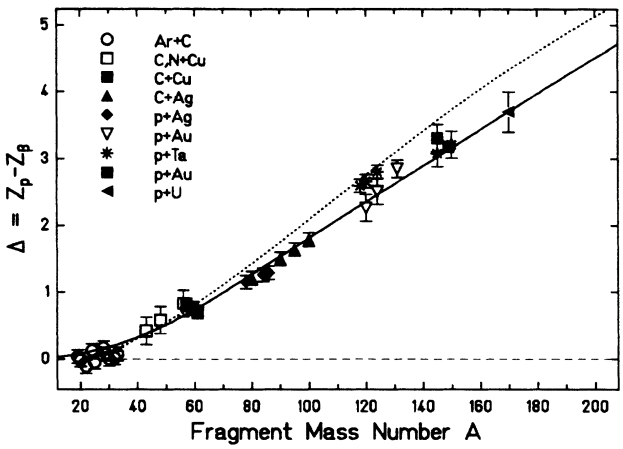

FIG. 5. Difference between the charge number at the maximum of the isobar distribution, Z_p, and the charge number at β-stability, Z_β, as a function of fragment mass for targets near the line of β-stability. Symbols denote experimental values derived from the literature (Ar+C: Ref. 26; C,N+Cu: Ref. 16; p,C+Ag: Ref. 17; p+Ta: Ref. 29; p+Au: Refs. 15,31; p+U: Ref. 28). The full line represents our fit to the data [Eq.(8)]. The most recent version of the Silberberg-Tsao formula (Ref. 21) is indicated with the dotted curve.

These three parameters are strongly correlated and difficult to obtain uniquely with a least-squares fitting technique. Therefore, we have chosen to fix the exponent U first and then analyze published data for Z_p and R.

(a) The parameter U. Rudstam[6] and Porile *et al.*[17] have used symmetric charge dispersions with values of the exponent U between 2 (a Gaussian curve) and 1.48. Other authors, however, have found that the charge distributions are asymmetric around their maxima.[16,20,21] Our analysis of the presently available data, including our low cross-section data from Table II (^{182}Ta,^{174}Lu,^{168}Tm), indicates that Rudstam's early suggestion that $U = 1.5$ gives a very good description of the neutron-rich side of the distribution, whereas the proton-rich side falls off like a Gaussian ($U = 2$). We have therefore chosen the parameter U to be

$$U = 2 \text{ for } (Z_p - Z) < 0 \text{ and } U = 1.5 \text{ for } (Z_p - Z) \geq 0. \quad (5)$$

This choice also nicely reproduces the data in the extreme wings of the distribution as is demonstrated below.

(b) The parameter Z_p. Conclusions drawn by previous authors from their analyses of fragmentation cross-sections can be summarized as follows: (i) The maxima of the charge distributions are always on the neutron-deficient side of the valley of β stability; (ii) for targets close to β stability Z_p is only a function of the fragment mass; and (iii) for more neutron-rich or neutron-deficient targets the fragments "remember" the neutron or proton excess of the target to varying extents (the so-called "memory effect"). We will discuss the case of targets close to β stability first and postpone temporarily the discussion of the memory effect.

Our parametrization of Z_p follows ideas developed by Chu *et al.*[28,29] i.e., the most probable charge, $Z_p(A)$, is measured relative to the β-stable charge, $Z_\beta(A)$:

$$Z_p(A) = Z_\beta(A) + \Delta. \quad (6)$$

To avoid the influence of shell effects in the calculation of Z_p, which are certainly washed out during the formation of the observed fragment by particle evaporation from the highly excited prefragment, $Z_\beta(A)$ is approximated by the smooth function:[30]

$$Z_\beta(A) = A/(1.98 + 0.0155A^{2/3}). \quad (7)$$

The difference, Δ, between experimental values of $Z_p(A)$ and $Z_\beta(A)$, is shown in Fig. 5 as a function of the fragment mass, A. As can be seen from Fig. 5, the variation of Δ is rather smooth for fragments from all targets between Ar and U. The residues from Ar fragmentation[26] have their distributions centered at the valley of β stability ($Z_p = Z_\beta$), whereas those from heavier targets have their centroids on the neutron-deficient side ($Z_p > Z_\beta$). The full line in Fig. 5 represents a fit to the data with a parabola describing the low-mass region and a line for the higher-mass region which are smoothly joined at fragment mass 66. This function is written

$$\Delta = \begin{cases} 2.041 \times 10^{-4} A^2 & \text{if } A < 66, \\ 2.703 \times 10^{-2} A - 0.895 & \text{if } A \geq 66. \end{cases} \quad (8)$$

Plotted the same way, the parametrization of Z_p by Silberberg, Tsao, and Letaw[21] shows a similar trend, although with a marked shift towards more neutron-deficient nuclei, especially for heavy fragments (dotted curve in Fig. 5).

It should be noted that other authors[32] arrived at a very similar dependence of Z_p on A as the one given above on the basis of a physical model which allows to physically interprete this dependence. Charity *et al.*[32] have performed extensive evaporation calculations of nuclei below $Z = 40$ over a wide range of excitation energies. They found that for sufficiently high excitation energies ($E^*/A > 1$ MeV) the locus of all evaporation residues could be parametrized as

$$A = 2.08Z_p + 0.0029Z_p^2 \tag{9}$$

which for $Z < 40$ is practically identical with our parametrization. This corroborates that the fragment distribution in relativistic heavy-ion collisions is to a large extent governed by evaporation of particles (and clusters) from highly excited prefragments.

(c) The width parameter R. Similar to the parameter Z_p just discussed, the width parameter R is a function of fragment mass only, irrespective of the target nucleus. This can be seen in Fig. 6, a plot of R versus fragment mass A for the reactions indicated in the figure. The data can be approximated with an exponential of the form

$$\ln R(A) = -6.770 \times 10^{-3} A + 0.778. \tag{10}$$

The dotted curve in Fig. 6 represents the function for R used by Rudstam[6] and also by Silberberg, Tsao, and Letaw[21] for heavy targets ($63 \leq A_t \leq 209$). There is a marked difference towards more narrow distributions compared to the data and the parametrization contained in Eq.(10). This will have a dramatic effect on the cross sections predicted for the exotic and most interesting isotopes that lie on the wings of the distribution.

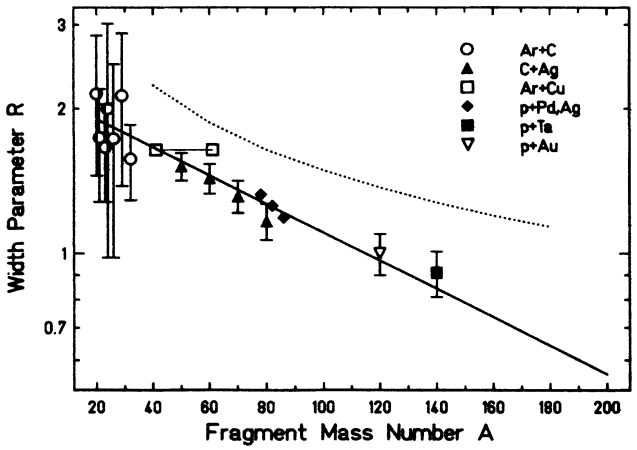

FIG. 6. Variation of the width parameter R of Eq.(1) with fragment mass. The symbols have the same meaning as in Fig. 5; additional data points for the reaction p+Pd,Ag (Ref. 33, diamonds) have been added later and indicate that our parametrization [Eq.(8), full line] is in very good agreement with experiment. The dotted curve gives the parametrization chosen by Rudstam (Ref. 6) and Silberberg, Tsao, and Letaw (Ref. 21).

We can summarize the considerations above in a concise form by stating that, for targets close to the line of β stability, the charge dispersion curve can be written as

$$\sigma(Z_p - Z) = n \exp(-R|Z_\beta + \Delta - Z|^U) \tag{11}$$

with the normalization factor $n = \sqrt{R/\pi}$ and R, Z_β, Δ, and U given by Eqs.(10), (7), (8), and (5), respectively. (We neglect the small error introduced by using the expression for n also on the neutron-rich side.)

(d) Influence of target neutron or proton excess. Most of the data used to derive empirical parametrizations of fragmentation cross sections have come from reactions with targets close to β stability. Because of the curvature of the valley of β stability, the neutron-to-proton ratio of the target, $(N/Z)_t$, increases with increasing target mass. It is reasonable to think that during the evaporation of particles from highly-excited primary fragments this neutron excess is partly lost due to the general preference for neutron emission (caused by the additional Coulomb barrier for proton emission). Nevertheless, residual nuclei from heavy targets are expected to be more neutron rich on average than those from light targets. Silberberg *et al.*[20,21] have taken this into account by subtracting a target-dependent factor from their function for Z_p that otherwise has only a fragment-mass dependence. Noguchi *et al.*[34] suggest a linear relationship correlating the fragment neutron-excess, $(N/Z)_p$, to the target neutron-excess, $(N/Z)_t$. This relationship has been established, however, only for the small range of fragments with $1.10 \leq (N/Z)_p \leq 1.27$.

We have followed a different approach: The "normal" memory effect for targets close to the line of β stability is accounted for in the expression $Z_p = Z_\beta + \Delta$ [Eq.(6)], through the variation of Z_β. Then Δ gives the shift of the most probable nucleus towards more neutron-deficient nuclei (caused by the evaporation process). What remains is finding a functional form for an additional shift, Δ_m, due to the neutron- or proton-excess of the target nuclei relative to the line of stability. This then leads to an expression for Z_p which reads

$$Z_p(A) = Z_\beta(A) + \Delta + \Delta_m. \tag{12}$$

Unfortunately, there are only two measurements in the literature on which to base such a description, the projectile fragmentation of ^{48}Ca at 212 MeV/nucleon[35] and the target fragmentation of ^{96}Ru, ^{96}Mo, and ^{96}Zr by 1.8 GeV protons.[36] We have used the ^{48}Ca data to deduce a function that describes the memory effect for a neutron-excess nucleus and then used the results of Porile and Church[36] as an independent check of our approach. Our ansatz is that the memory effect can be described by a shift of Z_p by a certain fraction of the distance of Z_t from β stability, while maintaining the shape of the isobar distribution. As in two-step models of fragmentation, we assume that the fractional shift is close to 1 near the target (resulting from prefragments with little excitation energy, consequently preserving any neutron excess of the target). The fractional shift gradually approaches zero

for fragments further away from the target as they stem from prefragments with higher excitation energies (and any neutron excess has been washed out in the evaporation process). This leads to the following expression:

$$\Delta_m(A) = [c_1(A/A_t)^2 + c_2(A/A_t)^4]\Delta_\beta(A_t) \qquad (13)$$

with $\Delta_\beta(A_t) = Z_t - Z_\beta(A_t)$ the distance of the target from the line of stability and Z_β is given by Eq.(7). The experimental values for Δ_m obtained from this analysis of the ^{48}Ca data by Westfall *et al.*[35] are displayed in the upper part of Fig. 7. The solid line corresponds to the parametrization of Eq.(13) with the constants

$$c_1 = 0.4 \text{ and } c_2 = 0.6. \qquad (14)$$

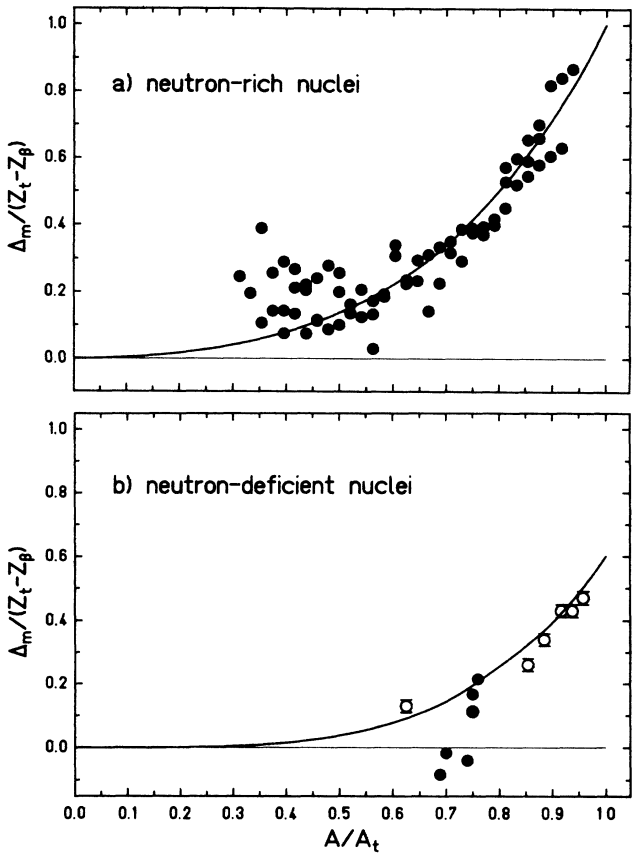

FIG. 7. Parametrization of the "memory effect" as explained in detail in Sec. IV C. Both axes are given in reduced units: the x axis represents the fragment-to-target mass ratio A/A_t; the y axis represents the additional shift Δ_m of the charge-dispersion curve divided by the target proton excess $\Delta_\beta = Z_t - Z_\beta$. The data points show how much the charge dispersion curve without memory effect, Eq.(11), has to be shifted to match an individual isotopic cross section from (a) the projectile-fragmentation of neutron-rich ^{48}Ca (Ref. 35); (b) the target-fragmentation of neutron-deficient ^{96}Ru (Ref. 36). The filled circles have been obtained from experimental cross sections, open circles have been obtained from analyzing internuclear-cascade calculations (this work). The thick lines represent polynomial fits to the data points [Eqs.(14) and (15)].

As anticipated above, the loss of memory develops gradually with increasing length of the evaporation chain. We regard this an important modification of other author's conclusions that the fragment N/Z-ratio depends only weakly on the target N/Z ratio.[1,34]

To illustrate the degree of agreement between this new description and data, Fig. 8 shows the measured charge distributions of mass-72 fragments from the reaction of 1.8 GeV protons with targets of ^{96}Ru, ^{96}Mo, and ^{96}Zr (Ref. 36). These three targets have widely varying values of $\Delta_\beta(A_t)$ of 2.35, 0.35, and -1.65, respectively [for reference, ^{48}Ca has a value of $\Delta_\beta(A_t)$ of -1.97]. We can conclude from Fig. 8 that (i) the shape of the isotope distributions, especially on the neutron-rich side (low Z numbers), is well reproduced by this parametrization, over more than three orders of magnitude; (ii) the parametrization of the memory effect fitted to the ^{48}Ca data is in good agreement with the data for the neutron-rich ^{96}Zr target; (iii) the fragment distribution for the neutron-deficient ^{96}Ru target deviates not very much from that of the ^{96}Mo target, irrespective of its large value of $\Delta_\beta = 2.35$. In order to obtain a reasonable guess for the parametrization of the memory effect on the neutron-deficient side, which is obviously smaller than on the neutron-rich side, we have (i) shifted the results from the reaction p+^{96}Ru in the same way as for ^{48}Ca, (ii) analyzed results for the ^{96}Ru target from internuclear cascade calculations (see Sec. IV E). The corresponding shift values are displayed as solid and open circles, respectively, in the lower part of Fig. 7. An approximate parametrization for these data in terms of Eq.(13) reads

$$c_1 = 0.0 \text{ and } c_2 = 0.6. \qquad (15)$$

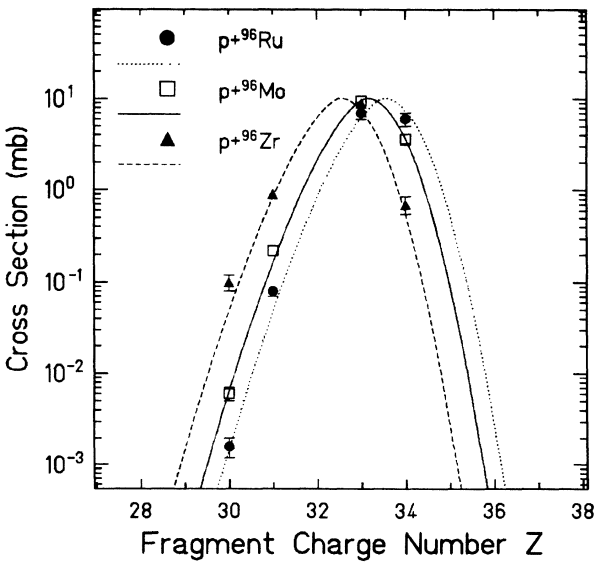

FIG. 8. Cross sections for A=72 isobars from the reaction of 1.8 GeV protons with ^{96}Ru, ^{96}Mo, and ^{96}Zr. The symbols are experimental data from the work of Porile and Church (Ref. 36). The curves are from our empirical description with the memory effect parametrized according to Eq.(13).

For the mass-72 fragments from the ^{96}Ru target shown in Fig. 8, this corresponds roughly to a memory effect of about one-half of that for the neutron-rich side.

In summary, the charge dispersion, including the memory effect, can be written as

$$\sigma(Z_p - Z) = n \exp(-R|Z_\beta + \Delta + \Delta_m - Z|^U) \qquad (16)$$

with the same notation as in Eq.(11) and the additional term, Δ_m, given by Eq.(13) with the constants c_1 and c_2 from Eqs.(14) and (15) for neutron-rich and neutron-deficient targets, respectively.

D. Comparison of experimental data with the empirical parametrization

In the following section we first want to demonstrate that the empirical parametrization described in the previous paragraph provides an excellent reproduction of measured cross sections for medium-mass targets. As an example, we have selected a comparison with data from the reactions of 28 GeV protons and 80 GeV ^{40}Ar ions with natural copper targets.[16] In Fig. 9 we display this comparison in the same way as in Ref. 16, namely, as a charge dispersion curve, where the experimental data are divided by their respective mass yields and plotted as a function of $Z_p - Z$. Thus one can display all data points, also for different projectiles, in comparison with one single calculated curve. As Fig. 9 shows, the agreement of our parametrization with the data points is very good. The fact that protons and argon ions produce the same charge dispersion has already been noted in Sec. IV B and is visualized by the close agreement between the circles and squares in Fig. 9.

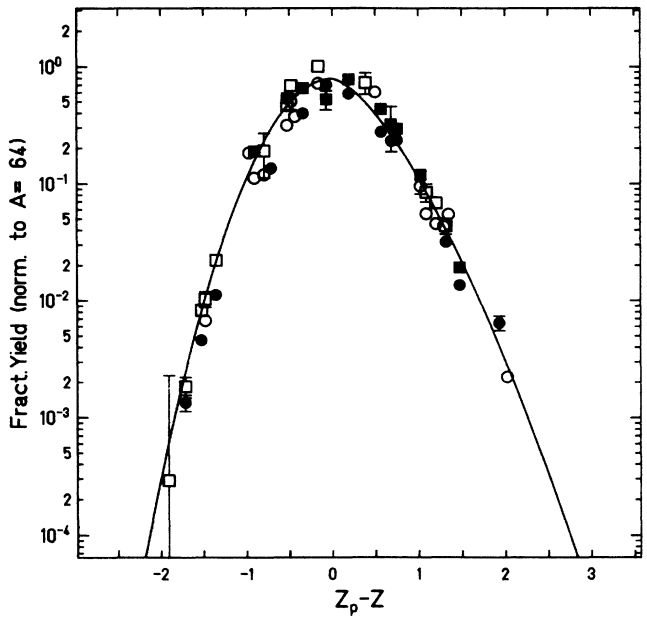

FIG. 9. Charge dispersion of fragments from the reaction of 28 GeV protons (circles) and of 80 GeV ^{40}Ar (squares) with ^{nat}Cu targets (Ref. 16). Open symbols denote cumulative cross sections, the full symbols indicate independent cross sections. The curve represents our empirical description, $\sigma(Z_p - Z)$, according to Eq.(1).

Next we want to address the question whether our empirical formula can also reproduce fragment cross-sections in the, up to now, largely unexplored mass region between $A \approx 150$ and $A \approx 200$. The present experiment lends itself well to such a comparison since we have measured a large number of *independent* cross-sections (at least on the neutron-rich side) not available from previous experiments with similar targets. For fragment masses around A=150, e.g., isotopes of the rare-earth elements Eu to Lu, the agreement is rather good. For fragments close to the Au target, however, the agreement becomes poorer as the fragment moves closer to the target. This can be seen from Fig. 10 where the thin curves indicate the Ir and Au isotope distributions calculated with the formulas described in the previous section. Obviously, the linear extrapolation of Δ as displayed in Fig. 5 is no longer valid very close to the target; the experimental isotope distributions are more neutron-rich. At the same time the slope on the neutron-rich side is reduced considerably, getting even positive for the Au isotope distribution, shown in the right-hand part of Fig. 10.

The clue as to how to modify the empirical formula to remove these discrepancies came from a close inspection of the results of internuclear-cascade (INC) calculations with the ISABEL code,[7] to be discussed in the next section. We had observed that INC calculations for the reaction of 8 GeV Ne ions with gold targets gave fragment distributions very similar in shape to our experimental results, differing in magnitude only by a constant factor of about 0.5 (dashed curves in Fig. 10). (We had to perform the calculations with light-ion instead of proton projectiles since an energy of 2.6 GeV/nucleon is beyond the limits of validity of the ISABEL code due to the neglect of multiple pion production in the model.) We have then investigated how to modify our formula, Eq.(1), in order to reproduce the shape of the near-target isobar distributions calculated with ISABEL. The most drastic modification is a shift of the centroid of the charge distribution towards β stability with decreasing mass loss from the target, reflected in a trend of the parameter Δ towards zero [Fig. 11(a)]. This shift towards β stability sets in at fragment masses of about 170 in the case of ^{197}Au as a target. At the same time, the width of the isobar distributions is reduced which is visualized by the rise of the parameter R [Fig. 11(b)]. We will discuss in Sec. IV E that such a trend is well in line with the physics underlying the INC model. To parametrize the observed features, we had to find a function that preserves the good agreement found for lighter fragments and gradually introduces the modifications when approaching the target as shown in Fig. 11. In analytical form, these functions can be written as multiplicative correction factors for the parameters Δ and R,

$$f_\Delta = -51(A/A_t - 0.86)^2 + 1 \qquad (17)$$

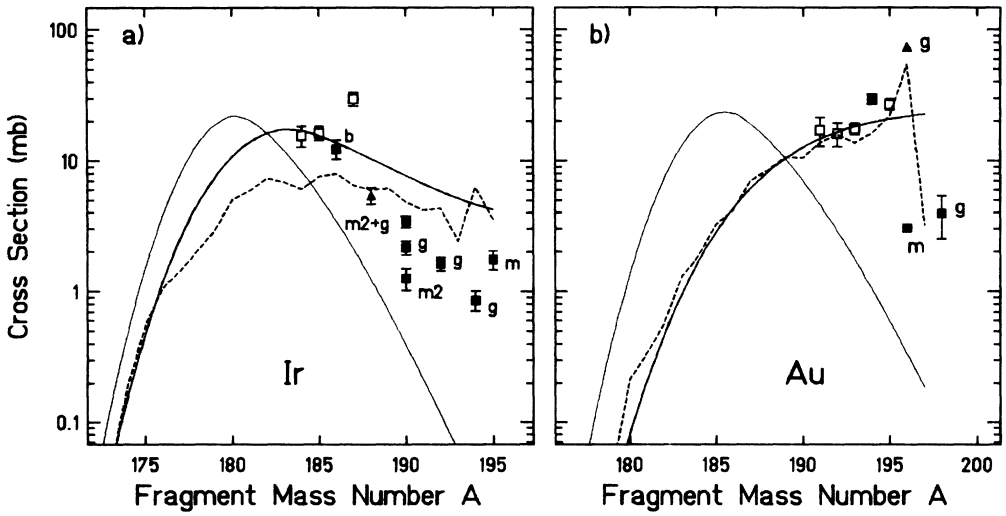

FIG. 10. Experimental cross sections for iridium and gold isotope distributions from ^{197}Au fragmentation. The data points are from this work (full squares: independent cross sections; open squares: cumulative cross sections; triangles: partially cumulative cross sections corrected for precursor contributions). The curves denote our empirical formula with extrapolated parameters (Sec. IV C, thin curves) and with modified parameters (Sec. IV D, thick curves). The dashed curves show the results of an internuclear-cascade calculation for the reaction of 8 GeV Ne ions with gold scaled down by the ratio of the (Ne+Au) to the (p+Au) mass yields (see text).

and

$$f_R = 20(A/A_t - 0.86)^2 + 1 \qquad (18)$$

for values of $A/A_t > 0.86$. These functions have the required property of approaching unity for $A/A_t \leq 0.86$. The resulting isotope distributions are indicated by the thick curves in Fig. 10; it is obvious that the agreement with the experimental data is much better. Good agreement is also found with one of the few previous measurements of independent cross sections of very heavy fragments where isotopic cross sections of gold isotopes have been determined after the bombardment of ^{209}Bi with C and Ne ions.[37] Careful inspection of near-target cross-sections from the reaction of protons with medium-mass targets also shows that in several cases the data are systematically better reproduced by the modified parameters, even though the improvement is less drastic than in the case of the gold or bismuth targets. For ^{nat}Cu and ^{nat}Ag targets, the target-dependent modifications of the parameters Δ and R are indicated by the dashed and dot-dashed lines in Fig. 11, respectively.

Our discussion of yields from the spallation of nuclei as heavy as gold implicitly assumes that the fissility of the target does not play an important role since it does not enter in any of the equations discussed above. This seems to be somewhat surprising since at projectile energies of several GeV one can assume that the excitation energy transferred to the target nucleus should grossly exceed the fission barriers which for ^{197}Au, e.g., are of the order of 20–25 MeV. On the other hand, experimental evidence has been accumulated that at high excitation energies the ratio of fission to particle evaporation is much smaller than calculated by conventional statistical models, e.g., in the case of 600 MeV proton-induced

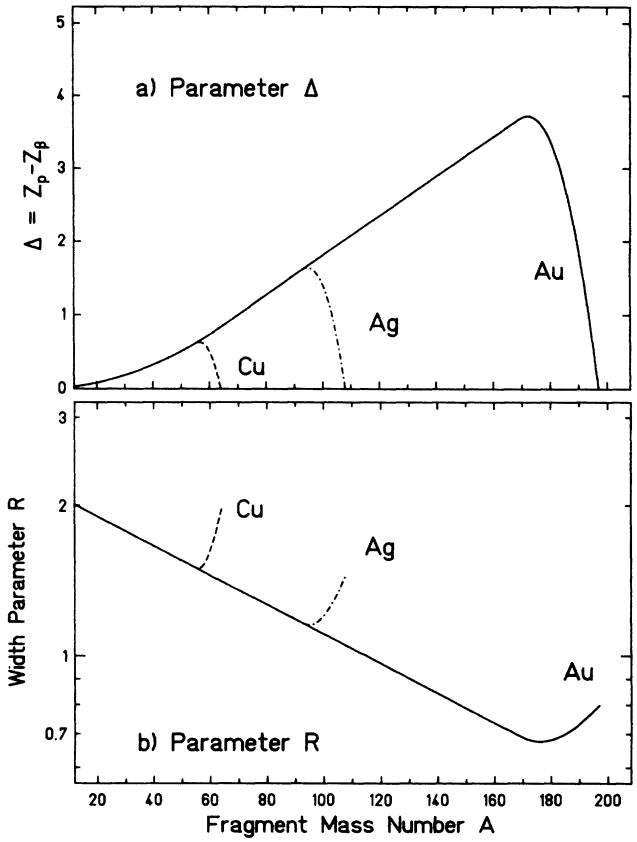

FIG. 11. (a) Difference Δ between the charge number at the maximum of the isobar distribution, Z_p, and the charge number at β stability, Z_β, for the fragmentation of copper, silver, and gold. The figure shows how the universal function for Δ [Eq.(8), Fig. 5], is modified for fragments close to the target by the multiplicative correction factor f_Δ, Eq.(17). (b) Same as (a) for the width parameter R. Here the correction factor f_R, Eq.(18), has been applied.

spallation of ^{232}Th (Ref. 38). Our experiment with a ^{232}Th target at 2.6 GeV proton energy was aimed at investigating if similar observations can be made at higher energies. As already discussed in Sec. III B, we have obtained several independent Au and one independent Tl isotope yield. The other cross sections measured are at least partially cumulative (see Table III). To compare these data with the empirical parametrization presented above, we have first normalized the formula to match the measured independent yields. This was to account for possible losses due to fission which is not included in our parametrization (assuming that all isotopes of an element are affected by fission competition to the same amount). The resulting normalization factor amounted to 0.4. Applying the same normalization factor to the respective precursor yields, we have then used the calculated cross sections to correct the measured partially-cumulative yields for β feeding during the irradiation and before the chemical separation. The results are shown in Fig. 12. One can see that with the normalization factor of 0.4 both the independent and corrected values are in good agreement with the empirical parametrization extrapolated from lighter nuclei. This has been verified, of course, only for the not so neutron-deficient nuclei on the right-hand side of the distributions; the situation may be different for the more neutron-deficient nuclei with smaller fission barriers on the left-hand side. It is interesting to note that the same survival factor of 0.4 has been found by Westmeier and Esterlund[38] in their experiment with 600 MeV protons on the same target. One can conclude that fission competition is not a severe obstacle in the production of neutron-rich trans-lead nuclei (at least close to β stability) by fragmentation of Th or U projectiles as foreseen at the GSI projectile-fragment separator, and that our empirical parametrization is a reasonable estimate for the yields of such nuclei if one allows for a factor of about 0.5 to account for fission losses.

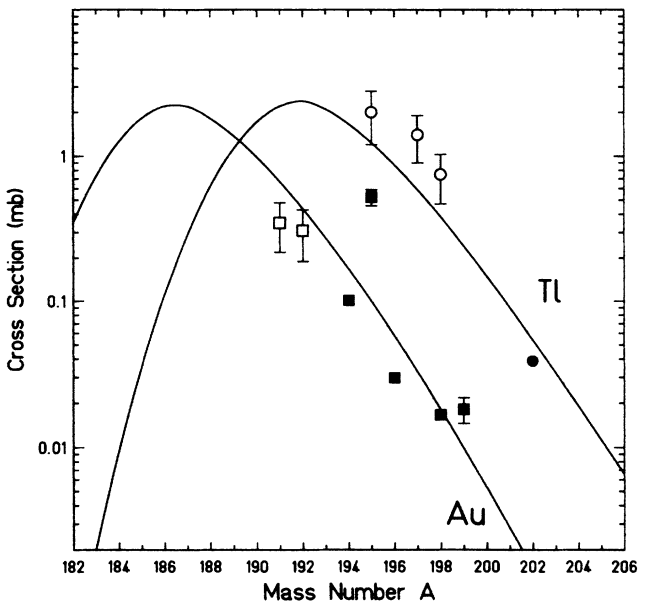

FIG. 12. Experimental cross sections of gold (squares) and thallium isotopes (circles) from the reaction of 2.6 GeV protons with a ^{232}Th target in comparison with the empirical parametrization discussed in the text. Full symbols denote independent cross sections. The curves represent isotopic yields from our parametrization multiplied by a factor of 0.4 to match the independent yields. The open symbols have been obtained by correcting measured partially cumulative cross sections (Table III) for their precursor contributions.

E. Comparison to internuclear-cascade calculations

Though the empirical approach presented so far allows to reproduce measured fragmentation cross-sections with sufficient accuracy (within a factor of 2 for about 85% of all available data), it would be more satisfactory to utilize a physical model that is able to calculate the cross sections with similar accuracy. Among the many models developed for high-energy hadron-nucleus collisions is the internuclear-cascade model ISABEL by Yariv and Fraenkel.[7] This model has been shown to reproduce successfully many aspects of high-energy reactions, e.g., inclusive particle spectra and angular distributions, multiplicity distributions, etc.[7] We have used an up-to-date version of this model[39] to perform some exploratory calculations of residual nuclei distributions. The spectrum of residual nuclei is certainly a less stringent test of an INC model calculation since this spectrum depends not only on the "fast" part of the reaction (the individual nucleon-nucleon collisions), but also on the "slow" part where nucleons or clusters are evaporated from the prefragments. The preceeding discussion of the general features of fragment distributions suggests that it is mainly the evaporation part which determines the final fragment distributions. In the ISABEL code evaporation is included in terms of the DFF code,[40] a Monte Carlo evaporation calculation which includes complex particle emission but ignores angular momentum.

Previously, detailed comparisons of measured fragment distributions with INC calculations have been made only for the case of ^{40}Ar fragmentation[41] where good agreement between theory and experiment has been observed. Similar comparisons with experimental data have been attempted for fragments from ^{nat}Ag (Ref. 7) and ^{181}Ta or ^{197}Au (Ref. 18) but were hampered by the lack of a sufficient number of measured independent cross sections. In the last case[18] the authors found a complete disagreement between experiment and INC calculations.

Our INC calculations have been performed with the standard options of the model. These options include folded-Yukawa density distributions for the colliding nuclei and the "slow rearrangement" option (for details of the different options, see Ref. 7). For light and medium-mass nuclei, typically 10^4 internuclear cascades were run. For heavy nuclei such as gold the increasing computer time needed per cascade limited the statistics to about 4000 cascades. Each prefragment produced in an inter-

nuclear cascade was subjected to 10 Monte Carlo evaporation calculations with the DFF evaporation code.

As illustrative examples of our calculations, we have selected the three cases of a light (Ar), a medium-mass (Ag), and a heavy nucleus (Au). The three reactions were (i) the projectile-fragmentation of 8 GeV ^{40}Ar with a C target[26]; (ii) the target-fragmentation of ^{nat}Ag with 12 GeV C (Ref. 17); (iii) the target-fragmentation of ^{197}Au with 8 GeV ^{20}Ne (Ref. 18). In all cases we compare the cross sections for a specific isotopic chain calculated with the INC model to our empirical parametrization. We have chosen our parametrization rather than the original experimental data for this comparison since we believe that this parametrization represents reasonably well the majority of the experimental cross-sections and thus is equivalent to a smoothing of the often scattered data points.

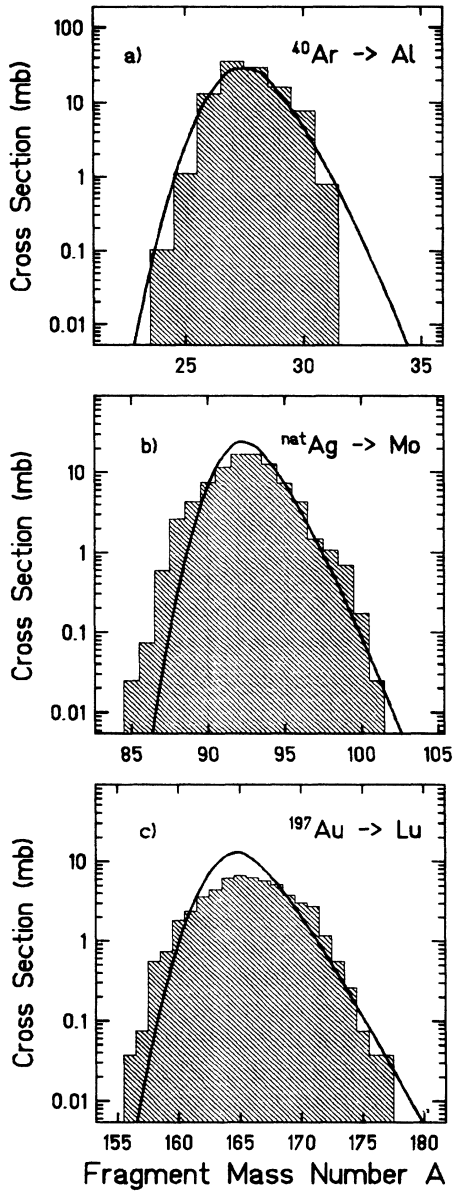

FIG. 13. Comparison between results from INC calculations with the Yariv-Fraenkel model (Ref. 7) (histograms) and our empirical parametrization (smooth curves). The examples shown represent (a) isotopic cross sections of Al isotopes from the projectile fragmentation of 8 GeV ^{40}Ar on ^{12}C, (b) same for Mo isotopes from 12 GeV ^{12}C on ^{nat}Ag targets, and (c) Lu cross sections from 8 GeV ^{20}Ne on ^{197}Au.

The comparison is shown in Fig. 13. As expected, the INC calculation and our curve agree well in the case of ^{40}Ar fragmentation [Fig. 13(a)]. Part (b) of Fig. 13 shows that also a medium-mass fragment distribution is well reproduced, particularly on the neutron-rich side. (It should be noted that further away from the Ag target the calculated INC fragment distributions are much wider than the experimental ones; this has already been noted by Porile *et al.*[17]) A surprisingly good agreement between our parametrization and the ISABEL calculation can be found in the case of gold fragments [Fig. 13(c)]. Though there is still a small difference in shape, both the position and the the width of the Lu isotope distribution shown agree with experiment, contrary to previous observations.[18] From the good agreement observed in the cases shown we conclude that the ISABEL code describes well both the fast and the slow part of a high-energy heavy-ion reaction even for heavy target nuclei.

The gross features of the fragment distribution resulting from an internuclear-cascade calculation of the target fragmentation of ^{197}Au can be seen best if we plot a two-dimensional representation of the isotopic cross-sections in the (A,Z) plane. This is done in Fig. 14. For clarity, we have plotted the results of the two reaction steps separately. In Fig. 14(a) we show the prefragment distribution after the fast (INC) step of the reaction. The resulting distribution is very narrow and closely concentrated around ^{197}Au. After the slow (evaporation) step of the reaction, a final fragment distribution results that is located mainly at the neutron-deficient side of the valley of β stability [the line of β stability is indicated by the dashed line in Fig. 14(b)]. Only close to the Au target nucleus, i.e. for small excitation energies, the fragments lie most probably close to β-stability. The full line in Fig. 14(b), which nicely coincides with the maxima of the calculated distribution, represents the line of the most probable charge, $Z_p(A)$, calculated according to Eq.(6); for ^{197}Au the memory effect is practically zero. Below fragment masses of $A_f = 170$ this line is given by the function for Δ extrapolated from lighter systems [Eq.(8); see Fig. 5]. For heavier fragment masses, the proton excess Δ according to Eq.(8) is replaced by Δf_Δ according to Eq.(17) which bends the full curve gradually towards β stability and towards the target nucleus, ^{197}Au.

V. SUMMARY AND CONCLUSIONS

By combining cross sections from this experiment (the reaction of 2.6 GeV protons with ^{197}Au and ^{232}Th) with data from the literature, we have been able to

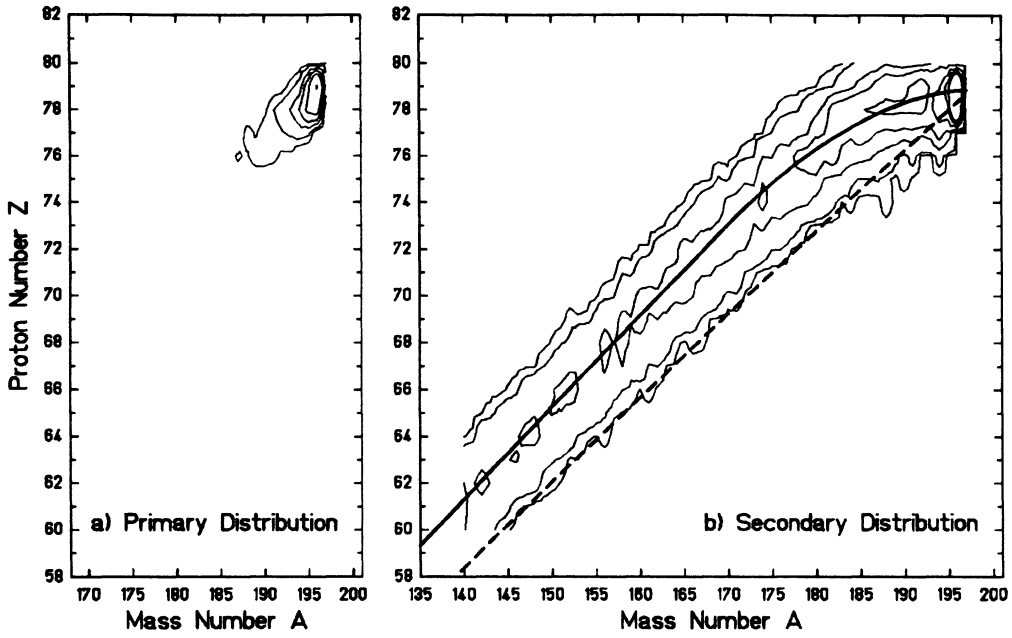

FIG. 14. Contour plots of isotopic cross sections calculated with the ISABEL internuclear-cascade model (Ref. 7) for the target-fragmentation of ^{197}Au induced by 8 GeV ^{20}Ne ions. Part (a) on the left-hand side shows the primary (prefragment) distribution resulting from the fast (INC) part of the reaction (contour lines represent cross sections from 20 to 200 mb). Part (b) on the right-hand side shows the secondary distribution after the slow (evaporation) part of the reaction; here the contours are drawn for cross sections between 0.3 and 40 mb. The dashed curve in (b) indicates the line of β stability [Eq.(7)], whereas the full curve represents the maxima of our empirical parametrization, $Z_p = Z_\beta + \Delta$, with Δ given by Eq.(8). Note how the correction factor f_Δ, Eq.(17), causes Z_p to approach β stability for small numbers of nucleons emitted from the Au target.

derive a new parametrization for fragmentation cross-sections of arbitrary target-projectile combinations. This parametrization was developed with an emphasis on heavy target (or projectile) nuclei and should be applicable for fragments from targets (or projectiles) with masses larger than approximately $A = 40$, provided the "limiting fragmentation" condition is fulfilled.

New features that have not been present in previous parametrizations of this type are (i) an analytical formula for the "memory effect," i.e., the influence of the target or projectile N/Z ratio on the fragment N/Z ratio; (ii) a modified parametrization of the proton-excess, Δ, in the vicinity of the original nucleus which drastically effects the cross sections of heavy fragments as the ones studied in the present work. Our parametrization allowed to reproduce approximately 85% of roughly 700 experimental fragment cross sections within a factor of 2.

We have confronted the results of our empirical description with the predictions of an internuclear-cascade calculation with the Yariv-Fraenkel model. We were able to demonstrate that qualitatively this model predicts the right position and width of the isotope distribution also for heavy nuclei.

ACKNOWLEDGMENTS

We would like to thank Dr. G. Milleret and Dr. M. Quechon of the Laboratoire National Saturne at Saclay for their help in performing the bombardments and Dr. P. Bourdinaud and Dr. N. Sautiez for the use of the chemical laboratory. Discussions of the internuclear-cascade model with Professor Z. Fraenkel are gratefully acknowledged. Two of us (D.J.M. and B.S.) would like to thank the staff of GSI and particulary the Kernchemie-I group for their hospitality during the course of the experiments. This work was supported by the Bundesministerium für Forschung und Technologie (Federal Republic of Germany).

*Permanent Address: Department of Chemistry, Michigan State University, East Lansing, Michigan 48824.

†Permanent Address: Institute of Experimental Physics, Warsaw University, 00-681 Warszawa, Poland.

‡Permanent Address: Insitute of Modern Physics, Academia Sinica, Lanzhou, People's Republic of China.

[1] J. Hüfner, Phys. Rep. **125**, 129 (1985).

[2] E.M. Friedlander and H.H. Heckmann, in *Treatise on Heavy Ion Science*, edited by D.A. Bromley (Plenum, New York, 1985), Vol. 4, p.403.

[3]J.P. Dufour, R. Del Moral, A. Fleury, H. Delagrange, and K.-H. Schmidt, Nucl. Instrum. Methods A **248**, 267 (1986).
[4]K.-H. Schmidt, E. Hanelt, H. Geissel, G. Münzenberg, and J.P. Dufour, Nucl. Instrum. Methods A **260**, 287 (1987).
[5]H. Geissel *et al.*, GSI Scientific Report 1988, Report No. GSI-89-1, 277, 1989, and references therein.
[6]G. Rudstam, Z. Naturforschung **21a**, 1027 (1966).
[7]Y. Yariv and Z. Fraenkel, Phys. Rev. C **20**, 2227 (1979).
[8]B. Szweryn, W. Brüchle, B. Schausten, and M.Schädel, Radiochimica Acta **47**, 33 (1989).
[9]U. Reus, W. Westmeier, and I. Warnecke, GSI Report No. 79-2, 1979.
[10]S.B. Kaufman and E.P. Steinberg, Phys. Rev. C **22**, 167 (1980).
[11]S.B. Kaufman, M.W. Weisfield, E.P. Steinberg, B.D. Wilkins, and D. Henderson, Phys. Rev. C **14**, 1121 (1976).
[12]J. Tobailem, C.H. de Lassus St.Genies, and L. Leveque, Report No. CEA-N-1-1466(1), 1971 (unpublished).
[13]Y. Asano, H. Kariya, S. Mori, M. Okano, and M. Sakano, J. Phys. Soc. Jpn. **57**, 2995 (1988).
[14]P. Adzic, private communication.
[15]K. Bächmann, J. Inorg. Nucl. Chem. **32**, 1 (1970).
[16]J.B. Cumming, P.E. Haustein, T.J. Ruth, and G.J. Virtes, Phys. Rev. C **17**, 1632 (1978); see also J.B. Cumming, R.W. Stoenner, and P.E. Haustein, *ibid.* **14**, 1554 (1976), and J.B. Cumming, P.E. Haustein, R.W. Stoenner, L. Mausner, and R.A. Naumann, *ibid.* **10**, 739 (1974).
[17]N.T. Porile, G.D. Cole, and C.R. Rudy, Phys. Rev. C **19**, 2288 (1979); G. English, N.T. Porile, and E.P. Steinberg, *ibid.* **10**, 2268 (1974).
[18]D.J. Morrissey, W. Loveland, M. de Saint Simon, and G.T. Seaborg, Phys. Rev. C **21**, 1783 (1980).
[19]S. Kox, A. Gamp, C. Perrin, J. Arvieux, R. Bertholet, J.F. Bruandet, M. Buenerd, R. Cherkaoui, A.J. Cole, Y. El-Masri, N. Longequeue, J. Menet, F. Merchez, and J.B. Viano, Phys. Rev. C **35**, 1678 (1987).
[20]R. Silberberg and C.H. Tsao, Astrophys. J. Suppl. **25**, 315 (1973); **25**, 335 (1973).
[21]R. Silberberg, C.H. Tsao, and J.R. Letaw, Astrophys. J. Suppl. **58**, 873 (1985); see also *Proceedings of the 20th International Cosmic Ray Conference*, Moscow, 1987, edited by V.L. Kozyarivsky (unpublished), Vol. 2, p. 133.
[22]W.R. Webber, J.C. Kish, and D.E. Schrier, Phys. Rev. C **41**, 520 (1990), and subsequent papers.
[23]D.L. Olson, B.L. Berman, D.E. Greiner, H.H. Heckman, P.J. Lindstrom, G.D. Westfall, and H.J. Crawford, Phys. Rev. C **24**, 1529 (1981).
[24]A.Y. Abul-Magd, W.A. Friedman, and J. Hüfner, Phys. Rev. C **34**, 113 (1986).
[25]L. Husain and S. Katcoff, Phys. Rev. C **7**, 2452 (1973).
[26]Y.P. Viyogi, T.J.M. Symons, P. Doll, D.E. Greiner, H.H. Heckman, D.L. Hendrie, P.J. Lindstrom, J. Mahoney, D.K. Scott, K. Van Bibber, G.D. Westfall, H. Wiemann, H.J. Crawford, C. McParland, and C.K. Gelbke, Phys. Rev. Lett. **42**, 33 (1979).
[27]J.C. Hill, F.K. Wohn, J.A. Winger, M. Khayat, and M.T. Mercier, Phys. Rev. C **39**, 524 (1989); M.T. Mercier, J.C. Hill, F.K. Wohn, C.M. McCullough, M.E. Nieland, J.A. Winger, C.B. Howard, S. Renwick, D.K. Matheis, and A.R. Smith, *ibid.* **33**, 1655 (1986).
[28]Y.Y. Chu, E.M. Franz, G. Friedlander, and P.J. Karol, Phys. Rev. C **4**, 2202 (1971).
[29]Y.Y. Chu, E.M. Franz, and G. Friedlander, Phys. Rev. C **10**, 156 (1974).
[30]P. Marmier and E. Sheldon, *Physics of Nuclei and Particles* (Academic, New York and London, 1971), Vol.I, p. 15.
[31]Y.W. Yu and N.T. Porile, Phys. Rev. C **12**, 938 (1975).
[32]R.J. Charity, D.R. Bowman, Z.H. Liu, R.J. McDonald, M.A. McMahan, G.J. Wozniak, L.G. Moretto, S. Bradley, W.L. Kehoe, and A.C. Mignerey, Nucl. Phys. **A476**, 516 (1988).
[33]B. Lavielle and S. Regnier, J. Phys. (Paris) **45**, 981 (1984).
[34]M. Noguchi, H. Hirabayashi, K. Katoh, K. Kondo, M. Takasaki, Y. Asano, S. Mori, and M. Sakano, Phys. Rev. C **38**, 1811 (1988).
[35]G.D Westfall, T.J.M. Symons, D.E. Greiner, H.H. Heckman, P.J. Lindstrom, J. Mahoney, A.C. Shotter, D.K. Scott, H.J. Crawford, C. McParland, T.C. Awes, C.K. Gelbke, and J.M. Kidd, Phys. Rev. Lett. **43**, 1859 (1979).
[36]N.T. Porile and L.B. Church, Phys. Rev. **133**, B310 (1964).
[37]K. Aleklett, D.J. Morrissey, W. Loveland, P.L. McGaughey, and G.T. Seaborg, Phys. Rev. C **23**, 1044 (1981).
[38]W. Westmeier and R.A. Esterlund, Z. Phys. A **316**, 27 (1984).
[39]Z. Fraenkel, private communication.
[40]I. Dostrovsky, Z. Fraenkel, and G. Friedlander, Phys. Rev. **116**, 683 (1959).
[41]D.J. Morrissey, L.F. Oliveira, J.O. Rasmussen, G.T. Seaborg, Y. Yariv, and Z. Fraenkel, Phys. Rev. Lett. **43**, 1139 (1979).